Biomedicine & Pharmacotherapy 148 (2022) 112769

Contents lists available at ScienceDirect

Biomedicine & Pharmacotherapy

journal homepage: www.elsevier.com/locate/biopha

NOD1 splenic activation confers ferroptosis protection and reduces macrophage recruitment under pro-atherogenic conditions

Victoria Fernández-García [a,b,*,1], Silvia González-Ramos [a,1], José Avendaño-Ortiz [c], Paloma Martín-Sanz [a,d], Carmen Delgado [a,b], Antonio Castrillo [a,e], Lisardo Boscá [a,b,*]

[a] Instituto de Investigaciones Biomédicas Alberto Sols (CSIC-UAM), Arturo Duperier 4, Madrid 28029, Spain
[b] Centro de Investigación Biomédica en Red en Enfermedades Cardiovasculares (CIBERCV), Monforte de Lemos 3–5, Madrid 28029, Spain
[c] Instituto de Investigación Sanitaria del Hospital Universitario La Paz, IdiPAZ. Pedro Rico, 6, Madrid 28029, Spain
[d] Centro de Investigación Biomédica en Red de Enfermedades Hepáticas y Digestivas (CIBERehd), Monforte de Lemos 3–5, Madrid 28029, Spain
[e] Unidad de Biomedicina (Unidad Asociada al CSIC), Instituto Universitario de Investigaciones Biomédicas y Sanitarias (IUIBS) de la Universidad de Las Palmas de Gran Canaria, Las Palmas, Spain

ARTICLE INFO

Keywords:
NOD1
Macrophages
Iron
Ferroptosis
CXCR2
Atherosclerosis

ABSTRACT

The bioavailability and regulation of iron is essential for central biological functions in mammals. The role of this element in ferroptosis and the dysregulation of its metabolism contribute to diseases, ranging from anemia to infections, alterations in the immune system, inflammation and atherosclerosis. In this sense, monocytes and macrophages modulate iron metabolism and splenic function, while at the same time they can worsen the atherosclerotic process in pathological conditions. Since the nucleotide-binding oligomerization domain 1 (NOD1) has been linked to numerous disorders, including inflammatory and cardiovascular diseases, we investigated its role in iron homeostasis. The iron content was measured in various tissues of *Apoe*$^{-/-}$ and *Apoe*$^{-/-}$*Nod1*$^{-/-}$ mice fed a high-fat diet (HFD) for 4 weeks, under normal or reduced splenic function after ligation of the splenic artery. In the absence of NOD1 the iron levels decreased in spleen, heart and liver regardless the splenic function. This iron decrease was accompanied by an increase in the recruitment of F4/80^{+}-macrophages in the spleen through a CXCR2-dependent signaling, as deduced by the reduced recruitment after administration of a CXCR2 inhibitor. CXCR2 mediates monocyte/macrophage chemotaxis to areas of inflammation and accumulation of leukocytes in the atherosclerotic plaque. Moreover, in the absence of NOD1, inhibition of CXCR2 enhanced atheroma progression. NOD1 activation increased the levels of GPX4 and other iron and ferroptosis regulatory proteins in macrophages. Our findings highlight the preeminent role of NOD1 in iron homeostasis and ferroptosis. These results suggest promising avenues of investigation for the diagnosis and treatment of iron-related diseases directed by NOD1.

1. Introduction

Iron is fundamental for the maintenance of life due to its contribution to essential metabolic and cellular processes (such as oxygen transport, energy production, detoxification or host defense); however, its dysregulation can lead to adverse effects, such as oxidative damage and ferroptosis. These processes are implicated in several chronic diseases such as inflammatory disorders and cardiovascular dysfunctions [1–3]. Indeed, iron homeostasis has also been related to immunometabolic and immune-related diseases, since iron dysregulation triggers alterations in immune cells and in the immune response [2].

Macrophages are essential for proper iron metabolism. They play important roles in erythropoiesis (by supplying iron), bacteriostasis (by sequestering this metal), erythrophagocytosis (especially by splenic macrophages, highlighting the importance of this organ) and modulation of tissue local iron bioavailability and function. To these aims, receptors such as CD163 (which is exclusively expressed in monocytes and macrophages and is related to the clearance of hemoglobin/haptoglobin complexes or to the detection of bacteria and the induction of local inflammation), and transporters like ferroportin 1 (FPN1; involved in iron export from cells) are indispensable [4–7].

Macrophages express pattern recognition receptors (PRRs), which

* Corresponding authors at: Instituto de Investigaciones Biomédicas Alberto Sols (CSIC-UAM), Arturo Duperier 4, Madrid 28029, Spain.
E-mail addresses: barbarav.fernandez@estudiante.uam.es (V. Fernández-García), lbosca@iib.uam.es (L. Boscá).
[1] These authors contributed equally to the work

https://doi.org/10.1016/j.biopha.2022.112769
Received 21 December 2021; Received in revised form 15 February 2022; Accepted 27 February 2022
Available online 3 March 2022

exert key functions in the innate immune response [8]; among them, nucleotide-binding oligomerization domain 1 (NOD1) plays essential roles in pathogen and damage recognition in macrophages and in the activation of critical immune responses [9–11]. The contribution of NOD1 to leukocyte mobilization, inflammation, metabolism and extramedullary hematopoiesis has been profusely characterized [12–15]. However, connections between iron metabolism, ferroptosis, specific leukocyte subset mobilizations and clinical data remain poorly defined. In addition, there are strong connections between iron homeostasis and cardiovascular diseases such as atherosclerosis [3,16–19]. Inflammation and oxidation are prominent mechanisms contributing to the complex process of atherogenesis, and iron leads to enhanced free radical production and ferroptosis [16,20]. These properties of iron mishandling added to hypercholesterolemia driven lipid mediated-oxidative stress can probably create synergies and potentiate atheroma development [21]. Indeed, iron affects all cell populations that actively participate in the atherosclerotic process (endothelial cells, vascular smooth muscle cells, platelets and monocytes/macrophages [17]). In this sense, it has been shown that the accumulation of iron in macrophages promotes the formation of foam cells and the development of atherosclerosis [22]. Furthermore, CXCR2 entails important roles in peripheral blood stem cell mobilization and recruitment of atherogenic and inflammatory monocytes. This receptor is expressed on neutrophils, but also on circulating endothelial progenitor cells (EPCs), fibroblasts, monocytes, macrophages and foam cells [23–25]. Indeed, it has been observed the binding of activated CXCR2 molecules to cholesterol, demonstrating the potential allosteric modulation function of cholesterol in chemokine receptors recognition [26]. However, beyond hypercholesterolemia, cell death is important in the atherosclerotic onset [27,28]. The cell death driven by loss of activity of the lipid repair enzyme glutathione peroxidase 4 (GPX4), which leads to the accumulation of reactive oxygen species (ROS) derived from fatty acids, mainly lipid hydroperoxides, has been termed ferroptosis. This iron-dependent cell death is markedly different from other forms of cell death, including regulated apoptosis, necrosis or necroptosis [1,20,29–32]. Ferroptosis has been investigated in depth in recent years due to its impact on degenerative disease, immunometabolic disorders and cancer. Small molecules can modulate the complex mechanisms involved in ferroptosis, thus offering novel opportunities for therapeutic interventions [1,33–35]. The aim of this work was to determine the role of NOD1 in iron metabolism and ferroptosis, especially its contribution to monocyte/macrophage function, as cells involved in the homeostasis of this metallic element.

2. Materials and methods

2.1. Human samples

Human peripheral blood mononuclear cells (PBMCs) were prepared from blood of healthy donors after information and written consent. The studies were approved by the Ethics Committee of La Paz hospital and were conducted in accordance with the Helsinki Declaration (project HULP PI-4100; approved April 2020). .

2.2. Animal procedures

All animal studies were firstly approved by the local ethics committee, and according to EU Directive 2010/63 and Recommendation 2007/526/EC in regard the protection of animals employed for experimental and other scientific purposes, enforced in Spanish law under Real Decreto 53/2013. *Apoe*$^{-/-}$ mice, bearing the C57BL/6 background, were obtained from Charles River (JAX mice stock #002052, Barcelona, Spain). Double-knockout *Apoe*$^{-/-}$*Nod1*$^{-/-}$ mice were generated by crossing *Apoe*$^{-/-}$ mice with *Nod1*$^{-/-}$ mice as previously described [14,15]. Briefly, *Apoe*$^{-/-}$*Nod1*$^{-/-}$ mice were generated by crossing *Apoe*$^{-/-}$ with *Nod1*$^{-/-}$ mice. Heterozygous mice were at the expected Mendelian ratios. Mice were genotyped by RT-PCR from ear samples. All assays compared male *Apoe*$^{-/-}$*Nod1*$^{-/-}$ mice *vs.* male *Apoe*$^{-/-}$ littermates.

For the spleen-involving surgeries, aiming to analyze the consequences of splenic loss of function, 3–4 mice per group were randomly assigned to either splenic hilar ligation or to control (sham). In short, animals were intubated and anesthetized with 2% isoflurane. The fur over the left side of the abdomen was shaved, mice were accommodated on a heating pad (37 °C) and skin was disinfected with alcohol and betadine before the intervention. The spleen was identified and it was ligated with a monofilament 7–0 nylon suture around the splenic arteries. The abdominal incision was carefully closed by using absorbable 5–0 sutures and specific glue for animal tissue (3 M™ Vetbond Tissue Adhesive). Ibuprofen (Dalsy) was supplied in drinking water (3 ml of medicine for every 250 ml of water) during 3 days after the procedure. Wound healing and adequate recovery after the surgical process were monitored daily. To accelerate the progression of atherosclerotic lesions and to establish a hypercholesterolemic onset, at 8 weeks of age and after sham operation or ligation of splenic arteries, mice males were kept on high-fat diet (HFD, 10.2% hydrogenated coconut oil, 0.75% cholesterol; Ssniff, Soest, Germany) for 4 weeks. Then, mice were anaesthetized intraperitoneally under general anesthesia (ketamine/xylazine combination at 80 mg/kg and 10 mg/kg body weight, respectively) before euthanasia by CO_2 inhalation. Whole blood was extracted *postmortem* by cardiac puncture and serum was obtained by initial blood coagulation and afterwards samples centrifugation at 1600g for 10 min at 4 °C. Total plasma cholesterol levels were determined to ensure the effect of the HFD (283 + 46 and 292 + 59 under chow diet, and 979 + 75 and 842 + 59 under HFD for *Apoe*$^{-/-}$ and *Apoe*$^{-/-}$*Nod1*$^{-/-}$ mice, respectively).

To conduct the CXCR2-blocking experiments, the CXCR2 inhibitor SB225002 (ref. SML0716; Sigma, Madrid, Spain) was administered intraperitoneally at 3 mg/kg, twice a week during the 4 weeks on HFD.

2.3. Iron and other basic elements content

Tissues (spleen, heart, liver) from mice on HFD were submitted to Inductively Coupled Plasma Mass Spectrometry (ICP-MS) measurements to determine the content in iron and other elements of interest. In brief, fresh tissues were firstly preserved at − 80 °C, then subjected to lyophilization and properly sealed and stored at 4ºC in a desiccator prior to submitting to the ICP protocol. ICP-MS equipment (ICP-MS NexION 300XX Perkin Elmer; Madrid, Spain) was used according to the manufacturer's instructions and specific treatments for these biological samples. Lyophilized tissues were submitted to acid digestion in a microwave oven adding 4 ml of HNO_3. Dissolved samples were graduated to a final volume of 25 ml in 1% HNO_3 (v/v). Samples were diluted 1:10 in 1% HNO_3 (v/v) and multi-element quantitative analysis were carried out.

2.4. Human cell procedures: monocytes

Human PBMCs were obtained from healthy donors´ freshly collected blood following previous protocols [36,37]. Monocytes were subjected to different stimuli in order to study NOD1 implication in iron metabolism. Cells were incubated for 1 h in medium supplemented with 400 μM $FeCl_3$ (Sigma) and then 1 h with 1 μg/ml of the FPN1 inhibitor ref. NBP1–21502PEP (Bionova, Madrid, Spain) or medium, plus 1 h with 1 μg/ml of the NOD1 agonist iEDAP (C12-iE-DAP, Invivogen, ref. tlrl-c12dap, San Diego, CA, USA). Afterwards, cells were washed with PBS and analyzed.

2.5. Mice cell procedures: peritoneal macrophages

Mice peritoneal macrophages were obtained from *Apoe*$^{-/-}$ and *Apoe*$^{-/-}$*Nod1*$^{-/-}$ mice peritoneal suspensions in the presence of DMEM (Sigma) plus 20% fetal bovine serum (FBS, Lonza; Basel, CH) and antibiotics (100 units/ml penicillin and 100 μg/ml streptomycin) as

previously described [38]. After seeding and washing with PBS to remove non-adherent cells, the culture was maintained for 24 h prior to use. The percentage of F4/80$^+$ cells was between 85% and 90%. Cells were treated with the NOD1 agonist iEDAP (1 μg/ml) or vehicle for 1 h. After removing the stimuli, macrophages were stimulated again with iron ($FeCl_3$; Sigma; used at 400 μM) for 24 h.

2.6. Flow cytometry assays

Mice blood and disaggregated spleen and bone marrow tissue were used for flow cytometry experiments. These assays were performed as previously described [14,15]. In summary, to analyze leukocyte populations, single cell suspensions were obtained after centrifugation and lysis (blood case) or flushing (spleen or femur and tibias) and they were prepared by processing the corresponding solutions through a 70 mm cell strainer. After 400g centrifugation for 5 min at 4 °C, the cell pellet was resuspended in HBSS (ThermoFisher, Waltham, MA, USA) supplemented with 10 mM Hepes and 0.5% bovine serum albumin (pH 7.4) and incubated for 30 min at 4 °C with: rat APC-Cy7-conjugated mAb against CD45 (1:200; BioLegend, ref. 47–0451; San Diego, CA, USA), rat PE-conjugated mAb against CD115 (1:100; BioLegend, ref. 135505), rat PerCpCy5.5- conjugated mAb against Ly6G (1:100; BioLegend, ref. 127616), rat FITC-conjugated mAb against Ly6C (1:100; BioLegend, ref. 128006), rat APC-conjugated mAb against F4/80 (1:100; BioLegend, ref. 123116), rat PECy7-conjugated mAb against Cd11b (1:100; ThermoFisher, ref. 25–0112), rat FITC-conjugated mAb against MHCII (1:100; BioLegend, ref. 205305), rat PE-conjugated mAb against MHCII (1:100; BD Biosciences, ref. 562010; Madrid, Spain), rat FITC-conjugated mAb against CD68 (1:100; BioLegend, ref. 137006), rat PE-conjugated mAb against CD169 (1:100; BioLegend, ref. 142402), rat FITC-conjugated mAb against CXCR2 (1:100; BioLegend, ref. 149608), rat PE-conjugated mAb against CCL2 (1:100; BioLegend, ref. 505904), rat PE-conjugated mAb against FPN1 (1:100; Novus Biologicals, ref. NBP1–21502PE), rat FITC-conjugated mAb against CD163 (1:100; ThermoFisher, ref. 11–1631), rabbit PE-conjugated pAb against GPX4 (1:100; Mybiosource, ref. MBS2069337). For cell counting, DAPI and absolute counting beads were used (Count-Bright; ThermoFisher; ref. C36950). Flow cytometry was conducted in a FACSCanto II (BD Biosciences), and cell subsets were defined using FlowJo software (Treestar, Ashland, OR, USA): leukocytes (CD45$^+$), neutrophils (CD45$^+$ CD11b$^+$ Ly6G$^+$), inflammatory monocytes (CD45$^+$ CD115$^+$ CD11b$^+$ Ly6C$^+$), patrolling monocytes (CD45$^+$ CD115$^+$ CD11b$^+$ Ly6C$^-$), tissue macrophages (CD45$^+$ F4/80$^+$), red pulp macrophages (RP) (CD45$^+$ F4/80$^+$ CD11b^{low} MHCII^{low}), white pulp macrophages (WP) (CD45$^+$ F4/80$^-$ CD68$^+$ CD11b$^-$), marginal zone macrophages (MZs) (CD45$^+$ F4/80$^-$ CD68$^-$) and metallophilic macrophages (Metallo.) (CD45$^+$ F4/80$^-$ CD68$^+$ CD169$^+$). The expression of CXCR2, CCL2, FPN1, CD163 and GPX4 was quantified in the main leukocyte subsets.

2.7. Serum iron measurement

Iron profile in serum was analyzed in the mice groups after 4 weeks of HFD. Serum iron levels, including ferrous iron (Fe^{2+}), ferric iron (Fe^{3+}) and total iron were quantified using the Abcam Iron Colorimetric Assay Kit (ab83366) as per the manufacturer's specifications.

2.8. Histological analysis and lesion quantification

Mice tissues for Prussian Blue (spleen, liver, heart), Masson's trichrome (spleen) or hematoxylin/eosin (H/E) staining were obtained as previously described [14,15]. Briefly, to confirm the differences in iron content in *Apoe*$^{-/-}$ and *Apoe*$^{-/-}$*Nod1*$^{-/-}$ mice (sham or splenic artery ligation animals), as shown by the ICP-MS technique, tissues were fixed in 4% paraformaldehyde in PBS and embedded in paraffin. The 5 μm (spleens and livers) and 8 μm (hearts) sections of tissues (Jung RM2055; Leica Microsystems), were deparaffinized and samples were then stained with Prussian Blue (Sigma Iron Stain kit; ref. HT20–1KT), using standard procedures. To analyze splenic collagen levels, mouse spleens were fixed in 4% paraformaldehyde for 24 h at 4 °C, passed through sucrose gradients at 10% and 20% (PBS supplemented with the sucrose), incubated 24 h in 30% sucrose, embedded in optimal cutting temperature, and cryopreserved at − 70 °C. Cryocut cross sections (5 μm) were evaluated for Masson's trichrome staining (Masson-Goldner staining kit, Sigma, ref. 1004850001) as per manufacturer's instructions. For the evaluation of the atherosclerotic lesion mice groups underwent CXCR2 inhibition plus 4 weeks on HFD, murine hearts were fixed and cryopreserved as spleens in the previous Masson's trichrome assays. Images of these histological techniques were captured in a Zeiss Axiophot microscope with a Plan-Neofluar 310/0.3 objective (Carl Zeiss, Oberkochen, Germany) and a DP70 camera (Olympus, Tokyo, Japan). To avoid specific biases due to potential differences in tissue shape, cross sections of the entire fragment of tissue were analyzed and averaged. Both the collagen content (spleens) and the planimetric area of atherosclerotic plaques (hearts) with or without CXCR2 inhibition were measured in pixels using ImageJ (NIH) and quantified.

2.9. Immunostaining

Immunofluorescence analysis was done as previously described [14,15]. Briefly, mice spleens and hearts were fixed overnight for 24 h at 4 °C, underwent sucrose gradients at 10% and 20% (PBS supplemented with the sucrose), incubated 24 h in 30% sucrose, embedded in optimal cutting temperature, and cryopreserved at − 80 °C. Then, they were sectioned into 5 μm (spleens) and 8 μm (hearts) sections with a microtome (Jung RM2055; Leica Microsystems). Cryo-Section samples slides were rehydrated, subjected to antigen retrieval in 10 mM citrate buffer (pH 6.0), blocked, and stained with antibodies specific for mouse CD68 (1:200; Bio-Rad, ref. MCA1957GA), CD169 (1:20; BioLegend, ref. 142404), CXCR2-AF647 (1:20; BioLegend, ref. 149306), Ly6G (1:100; Pharmingen, ref. 551459), CD163-FITC (1:20; ThermoFisher, ref. 11–1631), CD36-PE (1:20; Santa Cruz, ref. sc-13572), followed by secondary staining using standard procedures [39,40]. Secondary antibodies for immunofluorescence were Alexa Fluor 594–conjugated anti-rat (ThermoFisher), FITC-conjugated anti-rabbit (Sigma), Alexa Fluor 647–conjugated anti-rat (ThermoFisher). Afterwards, nuclei were counterstained with DAPI (ThermoFisher). Immunofluorescence staining of cryo-sections were then mounted in Prolong Gold Antifade mounting medium (ThermoFisher, ref. D1306). Primary control panel was performed with an appropriate isotype control IgG, and secondary controls incubations were performed in the absence of primary antibody. To perform TUNEL technology assays, same methodology was used added to TUNEL kit (In Situ Cell Death Detection Kit, Fluorescein, ref. 11684795910; Roche) manufacturer's specifications. A LSM710 confocal microscope with a Plan-Apochromat 325/0.8 oil immersion objective (Carl Zeiss, Oberkochen, Germany) was employed to capture images from the immunofluorescence stainings. Images were analyzed using ImageJ and were further processed for presentation with Zen2009 (Carl Zeiss) software.

2.10. Western blot analysis

Mice splenic samples for Western blotting were snap-frozen in liquid nitrogen and stored at − 80 °C. Subsequent processing was carried out according to previous works of this group [14,15]. In summary, protein extracts from mouse tissues were obtained using ice-cold 25 mM bicine, 150 mM sodium chloride (pH 7.6) (T-PER Tissue Protein Extraction Reagent; ThermoFisher) supplemented with phosphatase cocktail and protease inhibitors (Sigma). Afterwards, proteins were resolved on SDS-PAGE gels and were transferred to nitrocellulose membranes. Proteins were detected using rabbit pAb against TNF-α (1:1000; Abcam, ref. ab8348), rabbit pAb against CXCR2 (1:1000; Abcam, ref. ab14935), mouse mAb against α-tubulin (1:4000; Sigma, ref. T9026) and

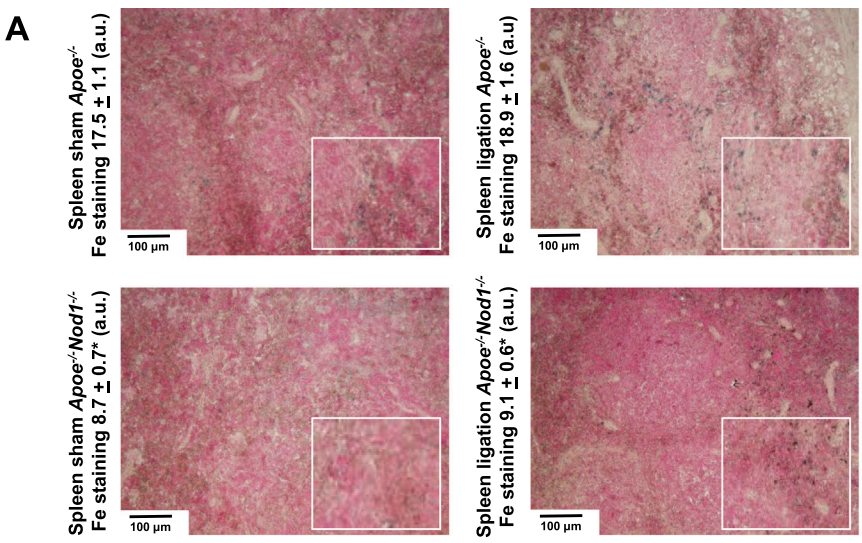

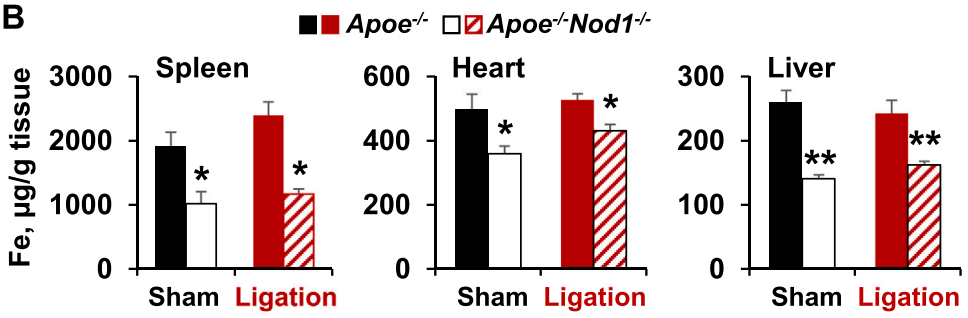

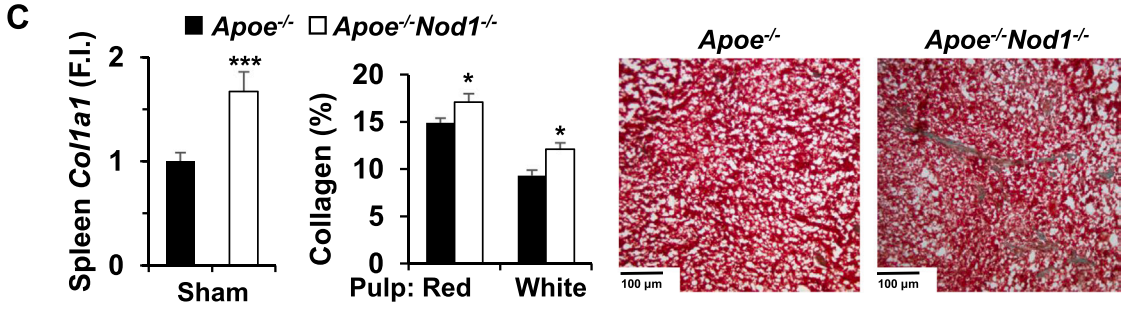

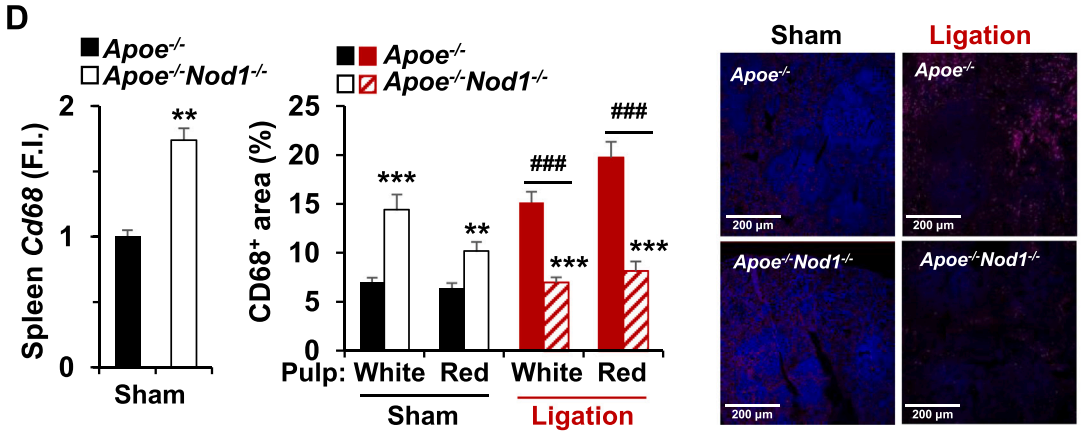

(caption on next page)

Fig. 1. NOD1 deficiency modifies iron homeostasis and splenic macrophage profile in *Apoe*$^{-/-}$ mice fed high-fat diet (HFD) for 4 weeks. (A) Representative images of spleens from sham and splenic artery ligation in male Apoe$^{-/-}$ and *Apoe*$^{-/-}$*Nod1*$^{-/-}$ mice for iron quantification (Prussian Blue). (B) Quantitative determination of iron content by ICP-MS in the spleen, liver and heart of sham and spleen artery ligation in *Apoe*$^{-/-}$ and *Apoe*$^{-/-}$*Nod1*$^{-/-}$ mice. (C) Quantification of splenic *Col1a1* mRNA, total collagen content (RP and WP) and representative images of Masson's trichrome staining from mice described in panel A. (D) *Cd68* mRNA levels in the spleen of sham *Apoe*$^{-/-}$ and *Apoe*$^{-/-}$*Nod1*$^{-/-}$ mice and immunofluorescence analysis of CD68^{+} cells and DAPI staining in splenic sections from *Apoe*$^{-/-}$ and *Apoe*$^{-/-}$*Nod1*$^{-/-}$ mice after sham or splenic artery ligation. Results show the mean + s.e.m. from 9 animals of each condition (*Apoe*$^{-/-}$ and *Apoe*$^{-/-}$*Nod1*$^{-/-}$, sham or splenic hilar ligation surgery). * $P < 0.05$; ** $P < 0.01$; *** $P < 0.005$ *vs.* the corresponding *Apoe*$^{-/-}$ or sham condition, or by 1-way ANOVA $^{\#}$ $P < 0.05$; $^{\#\#}$ $P < 0.01$; $^{\#\#\#}$ $P < 0.005$ when comparing splenic artery ligation with the corresponding sham condition in *Apoe*$^{-/-}$ or *Apoe*$^{-/-}$*Nod1*$^{-/-}$ mice. Bars: 100 μm (A, C); 100 μm (E). (A) Inset 4x magnification.(For interpretation of the references to colour in this figure, the reader is referred to the web version of this article.)

horseradish peroxidase–conjugated secondary antibodies (Bio-Rad). Protein bands were visualized using a Luminata chemiluminescence detection system (Merck) and an Image-Quant LAS 500 imager (GE Healthcare Life Sciences, Freiburg, Germany) and were quantified using ImageJ [National Institutes of Health (NIH), Bethesda, MD, USA]. Intensities of each protein bands were expressed as a percentage of those of the tubulin bands as indicated.

2.11. qRT-PCR

Total RNA was isolated by homogenization in QUIAZOL® by a TissueLyser LT and eluted using MinElute columns (Qiagen; Madrid, Spain). RNA integrity was assessed by RNA Nano Chip (Agilent Technologies; Madrid, Spain). 250 ng of RNA were retro-transcribed by using High-Capacity cDNA Reverse Transcription Kit (Applied Biosystems; Madrid, Spain). SYBR Green assay was conducted in a 7900HT Fast Real-Time PCR System equipment for qRT-PCR detection [14,15]. After performing the assays, calculations were obtained from measurement of technical triplicates of each sample. The relative amount of mRNA was calculated with the comparative $2^{-\Delta\Delta Ct}$ method using mouse or human *Hprt1* or *GAPDH*, respectively, as endogenous control transcripts. Murine and human sequences are given in Supplementary table S1.

2.12. Quantification and statistical analysis

To obtain the statistical analysis, GraphPad Prism 6 (GraphPad Software Inc.; San Diego, CA, USA) was used. All the values are expressed as means + s.e.m. Normality was calculated by D'Agostino–Pearson omnibus test, and afterwards a non-parametric test (Mann–Whitney U-test), or a normality test (unpaired Student's t test with Welch's correction, ordinary 1-wayANOVA) was used as appropriate in each case. Statistical significance was considered at P values < 0.05. Removal of outliers was carried out by ROUT method. Statistical tests and p values are showed for each panel in the corresponding figure legends. The number of individual animals for *in vivo* and *ex vivo* experiments is indicated in the figure legend.

3. Results

3.1. NOD1 activation affects iron homeostasis and macrophage recruitment in a splenic-dependent manner

The bioavailability of iron exerts adaptations in immune cells and the dysregulation of its metabolism favors significant alterations in the immune response, with the spleen being one of the relevant organs in its recycling. Quantification of iron content in the spleen of male *Apoe*$^{-/-}$ *vs.* *Apoe*$^{-/-}$*Nod1*$^{-/-}$ mice fed HFD for 4 weeks showed a significant decrease in splenic iron in NOD1 deficient animals (Fig. 1A-B). This decrease persisted after ligation of the splenic artery. Moreover, in addition to the spleen, a significant decrease in iron was also observed in the heart and in liver of *Apoe*$^{-/-}$*Nod1*$^{-/-}$ mice after accurate determination by ICP-MS (Fig. 1B). However, serum iron levels, including Fe^{2+}, Fe^{3+} did not show significant differences between mice genotypes (Suppl. Fig. S1A). Other key metal elements were determined in the same three tissues by ICP-MS; Na, Cu, Mg, K, Ca and Mn exhibited organ-specific changes depending on splenic artery ligation and the absence of NOD1. The most relevant result was the reduction of hepatic Cu levels in sham *Apoe*$^{-/-}$*Nod1*$^{-/-}$ mice (Suppl. Fig. S1B). As collagen levels and fibrosis have been related to iron metabolism in the spleen [41], we determined its content within this organ. *Col1a1* mRNA expression levels and splenic collagen content in white and red pulps were significantly increased under NOD1 deficiency (Fig. 1C).

Because splenic iron metabolism is regulated by different subsets of leukocytes, we analyzed the total and zonal distribution of inflammatory and patrolling monocytes under HFD; however, except for a modest increase in white pulp macrophages in *Apoe*$^{-/-}$*Nod1*$^{-/-}$ mice, no statistically significant differences were observed between other populations (Suppl. Fig. S2A). Furthermore, the splenic distribution of leukocytes was not significantly affected by NOD1 deficiency after splenic artery ligation (Suppl. Fig. S2B). Nevertheless, highlighting the involvement of monocytes/macrophages in these metabolic processes, *Cd68* expression was enhanced in the spleen of the sham *Apoe*$^{-/-}$*Nod1*$^{-/-}$ mice group. Immunofluorescence quantification of CD68 showed an increase in white and red pulps from *Apoe*$^{-/-}$*Nod1*$^{-/-}$ mice *vs.* *Apoe*$^{-/-}$. Ligation of the splenic artery showed an opposite trend (Fig. 1D). Splenic macrophages and marginal metallophilic macrophages were labelled with anti-Mac-3 or anti-CD169 antibodies, respectively, to visualize their distribution and confirm the white pulp organization (Suppl. Fig. S2C).

3.2. The NOD1/CXCR2 axis regulates macrophage mobilization and development of atherogenesis

Apoe$^{-/-}$*Nod1*$^{-/-}$ mice exhibited a significant increase in patrolling monocytes in the blood *vs.* *Apoe*$^{-/-}$ (Fig. 2A). In addition to this, circulating CD45^{+} myeloid cells (monocytes and neutrophils) were increased in *Apoe*$^{-/-}$*Nod1*$^{-/-}$ mice, whereas pharmacological activation of NOD1 with the agonist iEDAP in *Apoe*$^{-/-}$ mice significantly decreased these populations (Suppl. Fig. S3). Bone marrow assays indicated that the expression of the monocyte/macrophage biomarker *Cd68* was increased in *Apoe*$^{-/-}$*Nod1*$^{-/-}$ mice, independently of splenic artery ligation (Fig. 2B). These data suggested a different leukocyte mobilization that could contribute to modulate splenic iron metabolism. Firstly, we observed that the bone marrow mRNA levels of the transendothelial chemokine receptors *Cxcr2* and *Cxcr4* were decreased in sham *Apoe*$^{-/-}$*Nod1*$^{-/-}$ mice but upregulated after splenic artery ligation (Fig. 2C). In addition, CXCR2 exhibited the same trend in the spleen of sham *Apoe*$^{-/-}$ mice, in which TNF-α, accordingly to macrophage profile counts, was increased in *Apoe*$^{-/-}$*Nod1*$^{-/-}$ mice (Suppl. Fig. S4). Therefore, monocytes/macrophages recruitment appears to be associated with NOD1 activation under these conditions. Furthermore, flow cytometry assays of splenic cells showed differences between CD45^{+} subsets regarding the expression of CXCR2, especially in macrophages that exhibited enhanced CXCR2 expression in *Apoe*$^{-/-}$*Nod1*$^{-/-}$ mice, opposite to other splenic myeloid cells populations (Fig. 2D).

This role of CXCR2 in macrophage recruitment in the spleen of *Apoe*$^{-/-}$*Nod1*$^{-/-}$ mice was confirmed after *in vivo* pharmacological inhibition of this chemokine receptor (Fig. 2E). Interestingly enough, and because CXCR2 is known to be strongly expressed on macrophages within atherosclerotic lesions, inhibition of CXCR2 significantly increased atheroma formation in *Apoe*$^{-/-}$*Nod1*$^{-/-}$ mice (Fig. 2F). Moreover, immunofluorescence quantification of CD68 and Ly6G levels in the atherosclerotic lesion was similar (CD68) or even lower (Ly6G) in

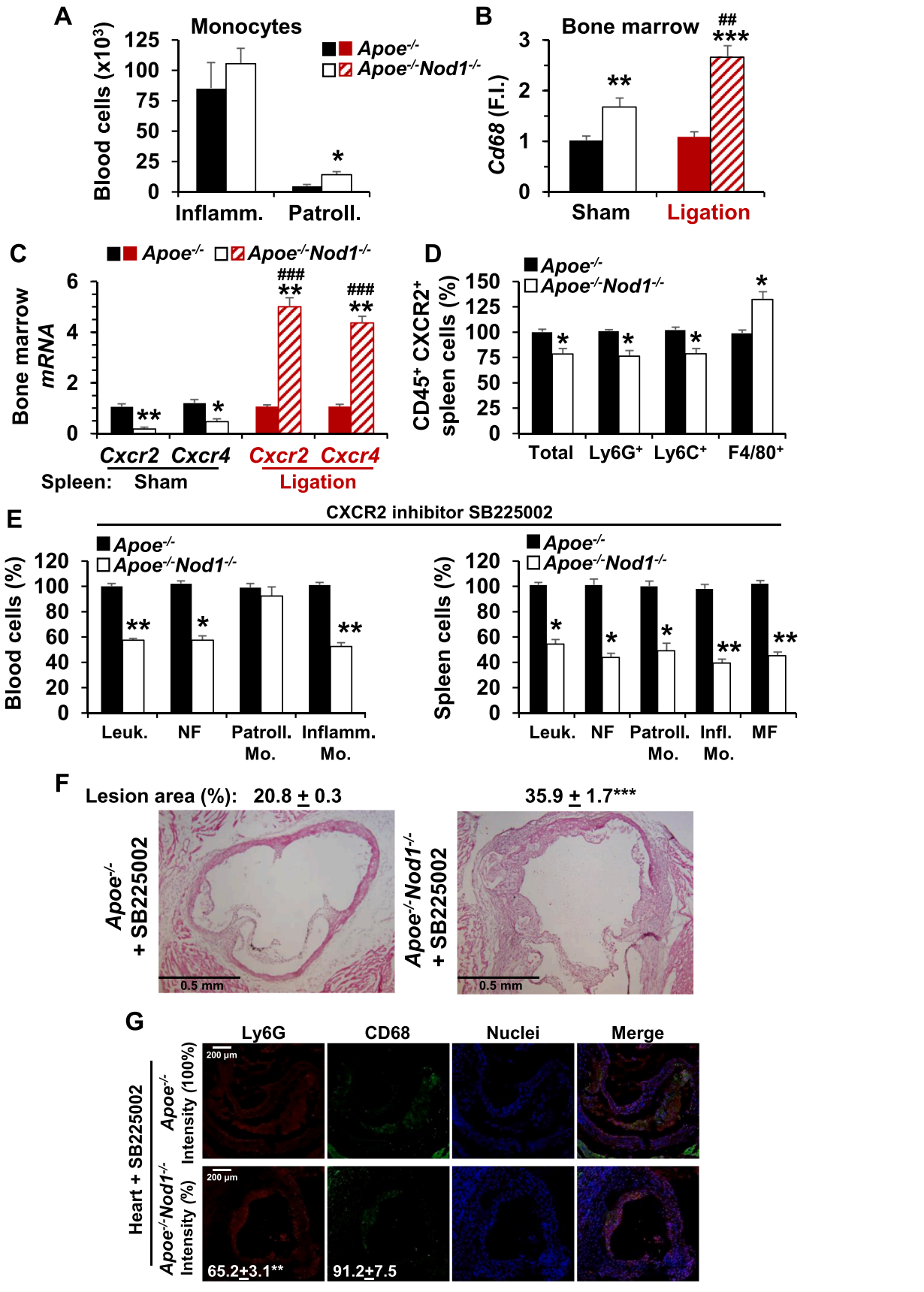

(caption on next page)

Fig. 2. NOD1 activation and CXCR2 modulation orchestrate monocyte and macrophage mobilization and influence atherogenesis under hypercholesterolemic conditions. (A) Quantification of circulating inflammatory and patrolling monocytes from spleen of sham *Apoe*$^{-/-}$ and *Apoe*$^{-/-}$*Nod1*$^{-/-}$ mice. (B) *Cd68* mRNA levels in the bone marrow of sham and splenic artery ligation of animals fed HFD. (C) *Cxcr2* and *Cxcr4* bone marrow mRNA levels from the same animals as in panel B. (D) Splenic CXCR2 expression in the main subsets of leukocytes from 4 weeks-fed HFD *Apoe*$^{-/-}$ and *Apoe*$^{-/-}$*Nod1*$^{-/-}$ mice. (E) Circulating and splenic leukocytes after CXCR2 inhibition (administered at 3 mg/kg twice a week during 4 weeks; HFD-fed). (F) Quantification and representative images of the atherogenic lesion in *Apoe*$^{-/-}$ and *Apoe*$^{-/-}$*Nod1*$^{-/-}$ mice from panel E. Analysis was performed after quantification of 6 consecutive sections of the lesion. (G) Quantification and representative images of immunofluorescences of LY6G, CD68 and nuclei (DAPI) in heart sections from panel E mice. Values were expressed as percentage *vs.* the sham *Apoe*$^{-/-}$ condition. Results show the mean + s.e.m. from 9 animals of each condition. * $P < 0.05$; ** $P < 0.01$; *** $P < 0.005$ *vs.* the corresponding intervention condition, or by 1-way ANOVA $^{\#\#\#}$ $P < 0.01$ when comparing splenic artery ligation with the corresponding sham condition in *Apoe*$^{-/-}$ or *Apoe*$^{-/-}$*Nod1*$^{-/-}$ mice. Bars: 0.5 mm (F); 200 μm (G).

Apoe$^{-/-}$*Nod1*$^{-/-}$ *vs. Apoe*$^{-/-}$ mice (Fig. 2G). These data demonstrate a link between NOD1 and CXCR2 modulation in macrophage recruitment in the athero-prone vascular context.

3.3. NOD1 contributes to the regulation of iron metabolism in macrophages

The above data prompted us to investigate the link between macrophage NOD1 activation under HFD and the regulation of iron homeostasis. Quantification in the bone marrow and spleen of *Ccl2* mRNA levels, one of the main chemokines that modulate the migration and infiltration of monocytes/macrophages, showed a significant increase in both tissue from *Apoe*$^{-/-}$*Nod1*$^{-/-}$ (Fig. 3A). However, splenic artery ligation reversed this upregulation of *Ccl2* in the bone marrow (Fig. 3A).

Relevant genes associated with iron metabolism were quantified in the spleen of sham mice: *Slc40a1* (encoding for FPN1, the main iron export transporter in macrophages), *Spic* (encoding for Spi-C, the transcription factor that regulates the development of red pulp macrophages needed for red blood cells recycling and iron metabolism) and *Slc7a11* (which exerts a critical role in the negative regulation of ferroptosis) were elevated in *Apoe*$^{-/-}$*Nod1*$^{-/-}$ mice. However, *Gpx4,* which represses ferroptosis, was downregulated in *Apoe*$^{-/-}$*Nod1*$^{-/-}$ mice (Fig. 3B). Iron-homeostasis related genes were analyzed in the liver of both sham and splenic artery ligation mice, as this organ is also highly involved in iron regulation. *Slc40a1*, *Hmox1*, *Col3a1* and *Prom2* showed the most remarkable changes. *Slc7a1* and *Prom2* levels were decreased after splenic artery ligation (Suppl. Fig. S5). Since FPN1 and CD163 are preeminent biomarkers in iron metabolism, they were determined in myeloid cells populations in spleen and blood. Splenic FPN1^{+} and CD163^{+} myeloid populations showed the greatest differences between mice groups (Fig. 3C). Interestingly, the only subsets with changes between mice genotypes in blood were that of FPN1^{+} and CD163^{+} monocytes, which were increased in the *Apoe*$^{-/-}$*Nod1*$^{-/-}$ group (Fig. 3D). Further analysis in sham mice spleens showed that CD68, CD163 and CD36 populations were highly increased in the red and white pulps of *Apoe*$^{-/-}$*Nod1*$^{-/-}$ mice (Fig. 3E).

3.4. NOD1 signaling affects ferroptosis in macrophages and spleen

Several proteins act as negative regulators of ferroptosis, including GPX4 and the cystine-glutamate antiporter (encoded by the *Slc7a11* gene). Having shown that *Gpx4* mRNA levels were decreased in *Apoe*$^{-/-}$*Nod1*$^{-/-}$ mice (Fig. 3B), analysis of GPX4 protein levels in splenic cells from *Apoe*$^{-/-}$ mice were higher than in *Apoe*$^{-/-}$*Nod1*$^{-/-}$ in almost all cell populations (Fig. 4A). Furthermore, CD68^{+} TUNEL^{+} cells were increased in the red pulp of *Apoe*$^{-/-}$*Nod1*$^{-/-}$ mice (Fig. 4B).

The role of NOD1 in macrophage ferroptosis was validated in peritoneal macrophages from *Apoe*$^{-/-}$ and *Apoe*$^{-/-}$*Nod1*$^{-/-}$ mice treated with iEDAP and iron enriched medium. As Fig. 4C shows, maximal activation of NOD1 significantly upregulated the expression of genes involved in protection against ferroptosis in *Apoe*$^{-/-}$ (*Slc40a1, Gpx4*, *Spic*, *Hmox1* and *Col1a1*). These genes were significantly decreased in peritoneal macrophages from *Apoe*$^{-/-}$*Nod1*$^{-/-}$ mice. In addition, these results were validated in human macrophages using the NOD1 agonist iEDAP and in the presence and absence of the FPN1 inhibitor NBP1–21502PEP. As Suppl. Fig. S6 shows, *NOD1*, *SLC40AA1* and the gene encoding for the ferritin light chain (*FTL*) mRNA levels were not affected under these conditions. However, *SPIC*, *CD163*, and *CD36* were repressed after FPN1 inhibition in cells treated with iEDAP. Other genes, such as *MCSF*, *LDLR, NFE2L2* (encoding for the transcription factor NRF2 involved in the defense against oxidative stress) and *HMOX1* were upregulated after iEDAP treatment, an effect that was not prevented by FPN1 inhibition.

4. Discussion

Iron metabolism and ferroptosis are involved in multiple biological processes [2,42,43] and macrophages play a role in the homeostatic handling and recycling of iron from senescent erythrocytes [2,4–7]. The present work aimed to study the role of NOD1 from splenic macrophage in these key processes. Our findings unveil a specific implication of NOD1 in iron dynamics through the regulation of FPN1, CD163 (the high-affinity receptor of haptoglobin-hemoglobin complexes) and GPX4 (protecting from ferroptosis) in the context of HFD. The connections between iron homeostasis and immune responses are well known [44–46] and here we demonstrate that NOD1 deletion causes a significant reduction in the iron content of essential organs (*e.g.*, spleen, liver and heart), and independent of partial loss of splenic function. It is worth mentioning that splenic artery ligation is a well-tolerated surgical intervention because, due to the vascular structure of the spleen, there is an extensive collateral blood supply to the organ [47].

Moreover, deficient iron bioavailability in these organs can lead to previously described severe chronic disorders [48–50].

The role of the spleen in iron storage and metabolism is well documented [51–53]. In this regard, collagen biosynthesis, for example, requires iron-dependent activities for the hydroxylation of the prolyl and lysyl residues that promote intermonomeric crosslinking leading to the formation of the classic triple helix collagen. Accordingly, reduced iron content in several organs (as occurs in the absence of NOD1) results in enhanced splenic transcription of the *Col1a1* gene and collagen accumulation, probably because of the reduced functional crosslinking required to maintain the correct structure of collagen fibrils, enhancing fibrosis and tissue damage [54]. In addition to this, increased levels of CCL2 in the bone marrow and spleen of NOD1-deficient animals under HFD conditions contribute to the pro-fibrotic role of this chemokine due to its ability to induce collagen production [55]. Moreover, *Ccl2* expression is crucial for monocyte mobilization and transmigration into the subendothelial space [1,56] and, precisely, they are remarkably enhanced in both the spleen and the bone marrow of *Apoe*$^{-/-}$*Nod1*$^{-/-}$ mice, the group with the highest splenic macrophage counts.

Macrophages play fundamental functions in wound healing mechanisms and collagen synthesis in several experimental models [57–61]. Our data show that, under HFD, splenic inflammatory and patrolling monocytes, precursors of tissue macrophages, exhibit changes between the mice genotypes. In addition, hilar splenic vessel ligation reverses the trend with respect to the content of patrolling monocytes and CD68^{+} macrophages in the red and white pulp. Moreover, the splenic levels of *Spic*, a transcription factor that controls the development of red pulp macrophages, which are in charge of iron homeostasis and red blood cells recycling, were enhanced in NOD1-deficient mice. Therefore, NOD1 activation by HFD is contributing to iron content, correct regulation of collagen synthesis (avoiding fibrosis), and splenic

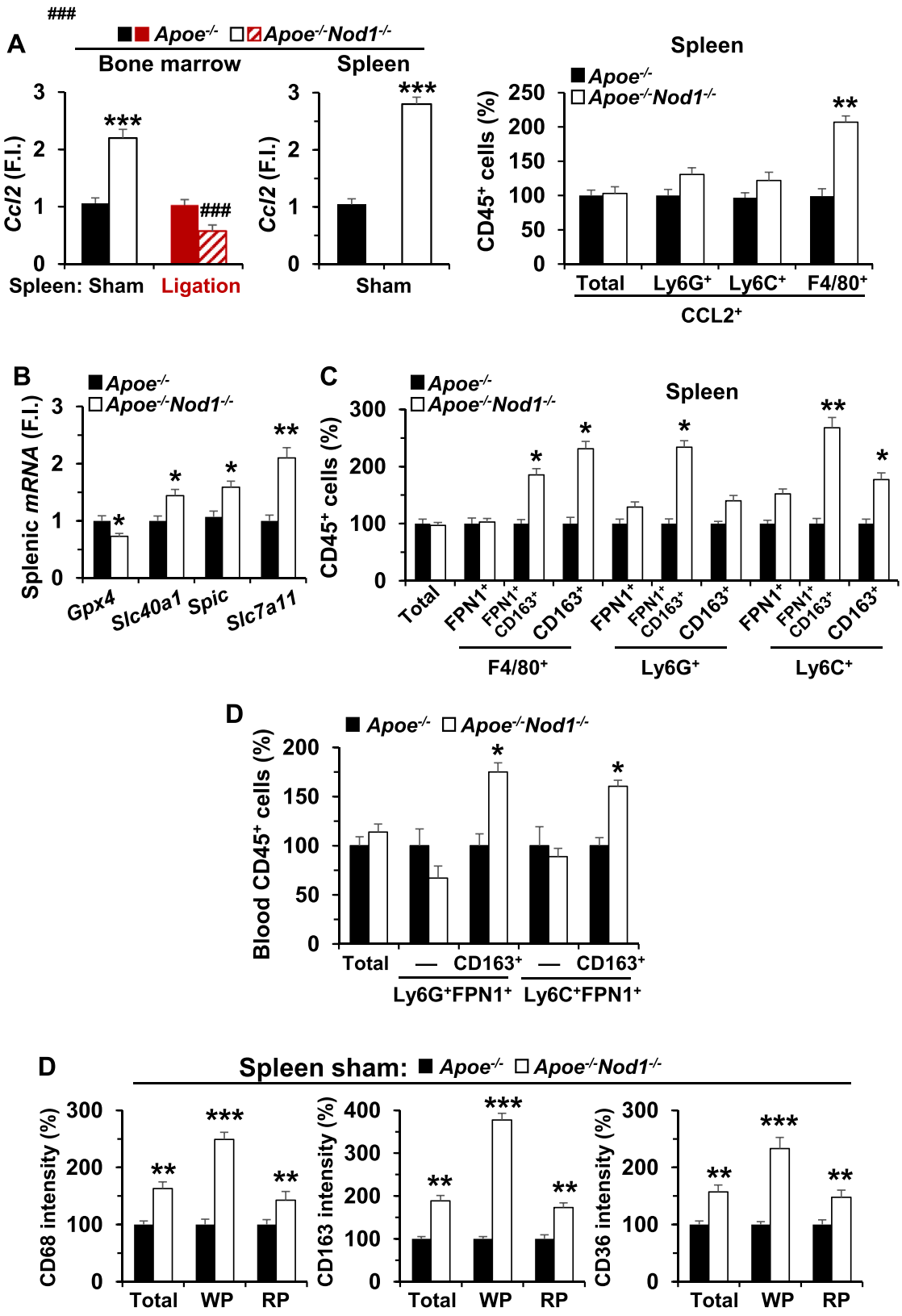

Fig. 3. NOD1 impairs iron metabolism in murine splenic macrophages and affects iron homeostasis in human monocytes. (A) Bone marrow and splenic mRNA levels of *Ccl2* in *Apoe*$^{-/-}$ and *Apoe*$^{-/-}$*Nod1*$^{-/-}$ mice (sham or after splenic artery ligation; *left panel*). Splenic CXCR2 expression in the main leukocyte populations (*right panel*). (B) Splenic mRNA levels of iron-related genes (*Gpx4*, *Slc40a1* (encoding for ferroportin 1, FPN1), *Spic* and *Slc7a11*. (C,D) Distribution of FPN1 and CD163 in the main myeloid cells populations in the spleen (C) and blood (D). (E) Immunofluorescence quantification of CD68, CD163 and CD36 staining in splenic sections from panel C. Results show the mean + s.e.m. from 9 animals of each condition. * $P < 0.05$; ** $P < 0.01$; *** $P < 0.005$ *vs.* the corresponding *Apoe*$^{-/-}$ condition, or by 1-way ANOVA. ### $P < 0.005$ when comparing splenic artery ligation with the corresponding sham condition in *Apoe*$^{-/-}$ or *Apoe*$^{-/-}$*Nod1*$^{-/-}$ mice.

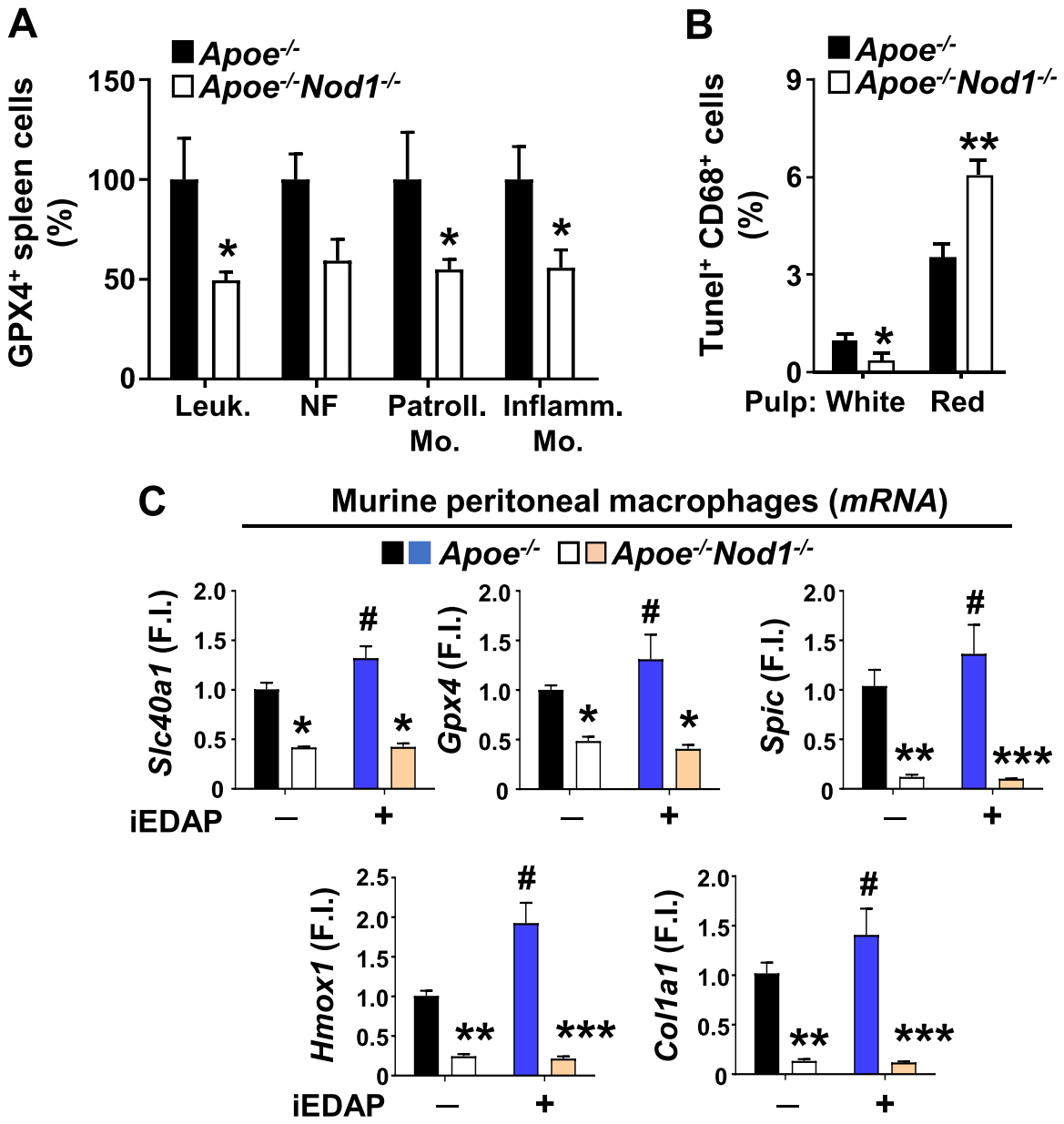

Fig. 4. NOD1 confers ferroptosis protection in mice fed HFD. (A) Quantification of splenic GPX4 levels in the main leukocyte populations. (B) $CD68^+$ and $TUNEL^+$ splenic cells from *Apoe*$^{-/-}$ and *Apoe*$^{-/-}$*Nod1*$^{-/-}$ mice. (C) mRNA levels of genes involved in iron homeostasis in murine peritoneal macrophages treated for 1 h with the NOD1 agonist iEDAP and 24 h with $FeCl_3$ (400 μM). Results show the mean + s.e.m. from 9 animals of each condition (sham and ligation of *Apoe*$^{-/-}$ and *Apoe*$^{-/-}$*Nod1*$^{-/-}$ mice). * $P < 0.05$; ** $P < 0.01$; *** $P < 0.005$ *vs.* the corresponding *Apoe*$^{-/-}$ condition; $^{\#}$ $P < 0.05$ *vs.* the condition in the absence of iEDAP.

monocyte/macrophage homeostasis.

Previous studies showed that splenic monocytes and macrophages contribute to atherosclerosis development [49], as well as to iron accumulation in atherosclerotic plaques [62]. Accordingly, our data show a higher iron content in the heart of *Apoe*$^{-/-}$ *vs.* *Apoe*$^{-/-}$*Nod1*$^{-/-}$ mice. In addition to this, the CXCL1/CXCR2 axis is key in classical HDF-induced monocytosis and neutralization of CXCL1 avoids the expansion of circulating monocytes [23]. Now, we show that CXCR2 inhibition reduces the splenic levels of macrophages in *Apoe*$^{-/-}$*Nod1*$^{-/-}$ mice, but favors the presence of circulating inflammatory cells that infiltrate the atherosclerotic lesion and promote its progression. These results agree with those by Dyer et al. [63], which demonstrated that exacerbated inflammation in the CXCR2-deficient mice was a consequence of altered myeloid cells recruitment.

Previous studies had shown a preeminent role for apoptotic neutrophils in triggering anti-inflammatory responses when interacting with macrophages [64]. In addition to this, our data show that TNF-α levels were notably increased in the spleens of *Apoe*$^{-/-}$*Nod1*$^{-/-}$ mice, in which CXCR2 was diminished. These results fit with previous studies describing that TNF-α down-regulates CXCR2 expression in human polymorphonuclear leukocytes and triggers its intravascular retention with an increased production of reactive oxygen species [65]. Moreover, a similar situation has been described after systemic infection by *S. aureus* [66].

Regarding CD163, it is expressed at high levels on splenic macrophages [6] and mediates the recovery of iron and iron-containing molecules [4]. This is consistent with the enhanced splenic levels of $CD163^+$ cells in *Apoe*$^{-/-}$*Nod1*$^{-/-}$ mice. Moreover, these data agree with the observed increase in the mRNA levels of genes involved in iron handling, such as *Slc40a1*, *Spic* and *Slc7a11* in NOD1-deficient mice. Indeed, NOD1 activation by iEDAP entails the polarization of macrophages to a pro-inflammatory phenotype, a condition that suppresses *Slc40a1*

transcription. Additionally, our results also agree with the fact that red pulp macrophages present high expression levels of Spi-C, the scavenger receptor CD163, heme oxygenase 1 (HO-1) and FPN1 [39,67,68]. All these molecules controlling iron bioavailability and preventing adverse oxidative effects.

As we have mentioned above, an excess of lipids leads to oxidative stress, lipid peroxidation and tissue damage; mechanisms that can be counteracted by antioxidant and anti-inflammatory proteins and enzymes such as HO-1 [69]. Interestingly, in iron-treated human monocytes stimulated with different agonists, it is worth mentioning that iEDAP-induced NOD1 stimulation leads to reduced expression of *HMOX1*, encoding for HO-1, a protein that has been associated with atheroprotection [55,70]. Moreover, *NFE2L2* is slightly overexpressed under iEDAP stimulation, in agreement with its known activation by cellular oxidative stress and noxious conditions [70,71]. However, it seems that the *NFE2L2*-dependent antioxidant-response is not capable of inducing sufficient HO-1 activity to alleviate the cellular stress and inflammation derived from the activation of NOD1 and the excess of iron. These results are in line with those previously published indicating that NOD1 deletion plays an atheroprotective role in early and advanced disease [14,15]. In fact, NOD1 activation in these iron-stimulated monocytes showed an increase in the expression of lipid responsive genes (*OLR1* and *LDLR*), while colony stimulating factor 1 (*CSF1*) was notably enhanced under the same conditions and especially when FPN1 was inhibited.

Finally, because GPX4 is at the crossroads of protection against peroxidation of membrane lipids, ferroptosis and antioxidant damage [32,72], we analyzed the role of this protein in the *Apoe*$^{-/-}$/*Nod1*$^{-/-}$ context. Not surprisingly, *Gpx4* levels were enhanced in the spleen of the *Apoe*$^{-/-}$ mice group, as it were also in the splenic main leukocyte subsets and in iron-stimulated peritoneal macrophages. These results, added to *Hmox1* enhanced expression in *Apoe*$^{-/-}$ peritoneal macrophages and assays showing that CD68^{+}-TUNEL^{+} cells were increased in the red pulp of NOD1-deficient mice, suggest that splenic cell death in *Apoe*$^{-/-}$*Nod1*$^{-/-}$ mice occurs *via* ferroptotic mechanisms. Indeed, NOD1 deficiency notably reduced apoptosis in peritoneal macrophages after iron supplementation. Therefore, we hypothesize that splenic NOD1 confers protection against ferroptosis in this organ to maintain leukocyte cells, mainly macrophages, in sufficient levels to mobilize them to inflammatory sites through systemic circulation and even recruit them to the atheroma layer. In this regard, extramedullary hematopoiesis plays a key role [73]. This idea is similar to that proposed for Gpx4 activity preventing lipid peroxidation and ferroptosis to sustain T*reg* cell activation and subsequent suppression of antitumor immunity [74].

5. Conclusion

Iron contributes to vital cellular and metabolic processes for the maintenance of health. This fact supposes that changes in its normal regulation can favor the development of severe pathophysiological processes. In this work we have demonstrated for the first time a clear link between immune player NOD1 and iron metabolism both in human and murine models. Moreover, the connections between ferroptosis, splenic activity modulation, atherosclerosis and leukocyte mobilization open novel multidisciplinary fields to explore, leading to identify potential pharmacological targets against different immune-metabolic diseases.

Funding sources

The experiments were performed in a laboratory where projects are supported by: Ministerio de Economía, Industria y Competitividad/Agencia Estatal de Investigación and Next Generation EU funds 10.13039/501100011033 (BIO2016–77639-P, PID2019–108977RB-I00 and PID2020–113238RB-I00), Centro de Investigación Biomédica en Red en Enfermedades Cardiovasculares (CB16/11/00222), Consorcio de Investigación en Red de la Comunidad de Madrid, S2017/BMD-3686 and Fondo Europeo de Desarrollo Regional and Fondo Solcial Europeo.

Author contributions

V.F.-G. wrote the paper, performed the experiments, designed the figures and revised the manuscript. S.G.-R. and J.A.O. provided experimental support, new ideas and improvements and revised the text. P. M.-S., A.C. and C.D. provided intellectual input. L.B. wrote and revised the manuscript, provided funding and intellectual input and discussed and organized the information.

Declaration of conflict of interest

The authors declare that they have no conflict of interest.

Appendix A. Supporting information

Supplementary data associated with this article can be found in the online version at doi:10.1016/j.biopha.2022.112769.

References

[1] J. Li, F. Cao, H. Yin, Z. Huang, Z. Lin, N. Mao, B. Sun, G. Wang, Ferroptosis: past, present and future, Cell Death Dis. 11 (2020) 88, https://doi.org/10.1038/s41419-020-2298-2.
[2] S.J.F. Cronin, C.J. Woolf, G. Weiss, J.M. Penninger, The role of iron regulation in immunometabolism and immune-related disease, Front. Mol. Biosci. 6 (2019), https://doi.org/10.3389/fmolb.2019.00116.
[3] A. Cornelissen, L. Guo, A. Sakamoto, R. Virmani, A.V. Finn, New insights into the role of iron in inflammation and atherosclerosis, EBioMedicine 47 (2019) 598–606, https://doi.org/10.1016/j.ebiom.2019.08.014.
[4] N.C. Winn, K.M. Volk, A.H. Hasty, Regulation of tissue iron homeostasis: the macrophage "ferrostat, JCI Insight 5 (2020), e132964, https://doi.org/10.1172/jci.insight.132964.
[5] T. Ganz, Macrophages and iron metabolism, Microbiol. Spectr. 4 (2016), https://doi.org/10.1128/microbiolspec.MCHD-0037-2016.
[6] M. Nairz, I. Theurl, F.K. Swirski, G. Weiss, "Pumping iron"-how macrophages handle iron at the systemic, microenvironmental, and cellular levels, Pflüg. Arch. Eur. J. Physiol. 469 (2017) 397–418, https://doi.org/10.1007/s00424-017-1944-8.
[7] M.P. Soares, I. Hamza, Macrophages and iron metabolism, Immunity 44 (2016) 492–504, https://doi.org/10.1016/j.immuni.2016.02.016.
[8] T.A. Seimon, A. Obstfeld, K.J. Moore, D.T. Golenbock, I. Tabas, Combinatorial pattern recognition receptor signaling alters the balance of life and death in macrophages, Proc. Natl. Acad. Sci. 103 (2006) 19794–19799, https://doi.org/10.1073/pnas.0609671104.
[9] N.E. Murugina, A.S. Budikhina, Y.A. Dagil, P.V. Maximchik, L.S. Balyasova, V. V. Murugin, M.V. Melnikov, V.S. Sharova, A.M. Nikolaeva, G.Z. Chkadua, B. V. Pinegin, M.V. Pashenkov, Glycolytic reprogramming of macrophages activated by NOD1 and TLR4 agonists: No association with proinflammatory cytokine production in normoxia, J. Biol. Chem. 295 (2020) 3099–3114, https://doi.org/10.1074/jbc.RA119.010589.
[10] L.O. Moreira, D.S. Zamboni, NOD1 and NOD2 signaling in infection and inflammation, Front. Immunol. 3 (2012) 328, https://doi.org/10.3389/fimmu.2012.00328.
[11] A.S. Budikhina, N.E. Murugina, P.V. Maximchik, Y.A. Dagil, A.M. Nikolaeva, L. S. Balyasova, V.V. Murugin, E.M. Selezneva, Y.G. Pashchenkova, G.Z. Chkadua, B. V. Pinegin, M.V. Pashenkov, Interplay between NOD1 and TLR4 receptors in macrophages: nonsynergistic activation of signaling pathways results in synergistic induction of proinflammatory gene expression, J. Immunol. 206 (2021) 2206–2220, https://doi.org/10.4049/jimmunol.2000692.
[12] S.L. Rivers, A. Klip, A. Giacca, NOD1: an interface between innate immunity and insulin resistance, Endocrinology 160 (2019) 1021–1030, https://doi.org/10.1210/en.2018-01061.
[13] S. Kanno, H. Nishio, T. Tanaka, Y. Motomura, K. Murata, K. Ihara, M. Onimaru, S. Yamasaki, H. Kono, K. Sueishi, T. Hara, Activation of an innate immune receptor, Nod1, accelerates atherogenesis in Apoe-/- mice, J. Immunol. 194 (2015) 773–780, https://doi.org/10.4049/jimmunol.1302841.
[14] S. Gonzalez-Ramos, M. Paz-Garcia, C. Rius, A. Del Monte-Monge, C. Rodriguez, V. Fernandez-Garcia, V. Andres, J. Martinez-Gonzalez, M.A. Lasuncion, P. Martin-Sanz, O. Soehnlein, L. Bosca, Endothelial NOD1 directs myeloid cell recruitment in atherosclerosis through VCAM-1, Faseb J. 33 (2019) 3912–3921, https://doi.org/10.1096/fj.201801231RR.
[15] S. González-Ramos, V. Fernández-García, M. Recalde, C. Rodríguez, J. Martínez-González, V. Andrés, P. Martín-Sanz, L. Boscá, Deletion or inhibition of NOD1 favors plaque stability and attenuates atherothrombosis in advanced atherogenesis, Cells 9 (2020) 2067, https://doi.org/10.3390/cells9092067.

[16] J. Auer, R. Berent, T. Weber, B. Eber, Coronary atherosclerosis and body iron stores, J. Am. Coll. Cardiol. 41 (2003) 1848–1849, https://doi.org/10.1016/S0735-1097(03)00325-5.

[17] P. Kraml, The role of iron in the pathogenesis of atherosclerosis, Physiol. Res. (2017) S55–S67, https://doi.org/10.33549/physiolres.933589.

[18] J.L. Sullivan, Iron in arterial plaque: a modifiable risk factor for atherosclerosis, Biochim. Biophys. Acta - Gen. Subj. 1790 (2009) 718–723, https://doi.org/10.1016/j.bbagen.2008.06.005.

[19] F. Vinchi, G. Porto, A. Simmelbauer, S. Altamura, S.T. Passos, M. Garbowski, A.M. N. Silva, S. Spaich, S.E. Seide, R. Sparla, M.W. Hentze, M.U. Muckenthaler, Atherosclerosis is aggravated by iron overload and ameliorated by dietary and pharmacological iron restriction, Eur. Heart J. 41 (2020) 2681–2695, https://doi.org/10.1093/eurheartj/ehz112.

[20] W.S. Yang, B.R. Stockwell, Ferroptosis: death by lipid peroxidation, Trends Cell Biol. 26 (2016) 165–176, https://doi.org/10.1016/j.tcb.2015.10.014.

[21] M.K. Chang, C. Bergmark, A. Laurila, S. Hörkkö, K.H. Han, P. Friedman, E. A. Dennis, J.L. Witztum, Monoclonal antibodies against oxidized low-density lipoprotein bind to apoptotic cells and inhibit their phagocytosis by elicited macrophages: evidence that oxidation-specific epitopes mediate macrophage recognition, Proc. Natl. Acad. Sci. U.S.A 96 (1999) 6353–6358, https://doi.org/10.1073/pnas.96.11.6353.

[22] J. Cai, M. Zhang, Y. Liu, H. Li, L. Shang, T. Xu, Z. Chen, F. Wang, T. Qiao, K. Li, Iron accumulation in macrophages promotes the formation of foam cells and development of atherosclerosis, Cell Biosci. 10 (2020) 137, https://doi.org/10.1186/s13578-020-00500-5.

[23] M. Drechsler, J. Duchene, O. Soehnlein, Chemokines control mobilization, recruitment, and fate of monocytes in atherosclerosis, Arterioscler. Thromb. Vasc. Biol. 35 (2015) 1050–1055, https://doi.org/10.1161/ATVBAHA.114.304649.

[24] L.M. Pelus, S. Fukuda, Peripheral blood stem cell mobilization: the CXCR2 ligand GRObeta rapidly mobilizes hematopoietic stem cells with enhanced engraftment properties, Exp. Hematol. 34 (2006) 1010–1020, https://doi.org/10.1016/j.exphem.2006.04.004.

[25] E. Rigamonti, C. Fontaine, B. Lefebvre, C. Duhem, P. Lefebvre, N. Marx, B. Staels, G. Chinetti-Gbaguidi, Induction of CXCR2 receptor by peroxisome proliferator-aActivated receptor γ in human macrophages, Arterioscler. Thromb. Vasc. Biol. 28 (2008) 932–939, https://doi.org/10.1161/ATVBAHA.107.161679.

[26] K. Liu, L. Shen, M. Wu, Z. Liu, T. Hua, Structural insights into the activation of chemokine receptor CXCR2, FEBS J. 289 (2022) 386–393, https://doi.org/10.1111/febs.15865.

[27] W. Martinet, I. Coornaert, P. Puylaert, G.R.Y.De Meyer, Macrophage death as a pharmacological target in atherosclerosis, Front. Pharmacol. 10 (2019) 306, https://doi.org/10.3389/fphar.2019.00306.

[28] K.J. Rayner, Cell death in the vessel wall, Arterioscler. Thromb. Vasc. Biol. 37 (2017) e75–e81, https://doi.org/10.1161/ATVBAHA.117.309229.

[29] M. Aldrovandi, M. Conrad, Ferroptosis: the good, the bad and the ugly, Cell Res 30 (2020) 1061–1062, https://doi.org/10.1038/s41422-020-00434-0.

[30] U.N. Das, Saturated fatty acids, MUFAs and PUFAs regulate ferroptosis, Cell Chem. Biol. 26 (2019) 309–311, https://doi.org/10.1016/j.chembiol.2019.03.001.

[31] L. Magtanong, P.-J. Ko, M. To, J.Y. Cao, G.C. Forcina, A. Tarangelo, C.C. Ward, K. Cho, G.J. Patti, D.K. Nomura, J.A. Olzmann, S.J. Dixon, Exogenous monounsaturated fatty acids promote a ferroptosis-resistant cell state, Cell Chem. Biol. 26 (2019) 420–432, https://doi.org/10.1016/j.chembiol.2018.11.016.

[32] G.C. Forcina, S.J. Dixon, GPX4 at the crossroads of lipid homeostasis and ferroptosis, Proteomics 19 (2019), e1800311, https://doi.org/10.1002/pmic.201800311.

[33] B.R. Stockwell, X. Jiang, The chemistry and biology of ferroptosis, Cell Chem. Biol. 27 (2020) 365–375, https://doi.org/10.1016/j.chembiol.2020.03.013.

[34] B.R. Stockwell, X. Jiang, W. Gu, Emerging mechanisms and disease relevance of ferroptosis, Trends Cell Biol. 30 (2020) 478–490, https://doi.org/10.1016/j.tcb.2020.02.009.

[35] M. Conrad, D.A. Pratt, The chemical basis of ferroptosis, Nat. Chem. Biol. 15 (2019) 1137–1147, https://doi.org/10.1038/s41589-019-0408-1.

[36] A. Povo-Retana, M. Mojena, A.B. Stremtan, V.B. Fernández-García, A. Gómez-Sáez, C. Nuevo-Tapioles, J.M. Molina-Guijarro, J. Avendaño-Ortiz, J.M. Cuezva, E. López-Collazo, J.F. Martínez-Leal, L. Boscá, Specific effects of trabectedin and lurbinectedin on human macrophage function and fate—novel insights, Cancers (Basel) 12 (2020) 3060, https://doi.org/10.3390/cancers12103060.

[37] M. Rola-Pleszczynski, W.H. Churchill, Purification of human monocytes by continuous gradient sedimentation in ficoll. J. Immunol. Methods 20 (1978) 255–262, https://doi.org/10.1016/0022-1759(78)90260-0.

[38] J.-C. Rodríguez-Prados, P.G. Través, J. Cuenca, D. Rico, J. Aragone, P. Martín-Sanz, M. Cascante, L. Boscá, Substrate fate in activated macrophages: a comparison between innate, classic, and alternative activation, J. Immunol. 185 (2010) 605–614, https://doi.org/10.4049/jimmunol.0901698.

[39] N. A-Gonzalez, A. Castrillo, Origin and specialization of splenic macrophages, Cell. Immunol. 330 (2018) 151–158, https://doi.org/10.1016/j.cellimm.2018.05.005.

[40] Á. Sánchez, M.C. Orizaola, D. Rodríguez-Muñoz, A. Aranda, A. Castrillo, S. Alemany, Stress erythropoiesis in atherogenic mice, Sci. Rep. 10 (2020) 18469, https://doi.org/10.1038/s41598-020-74665-x.

[41] A. Bellomo, R. Gentek, R. Golub, M. Bajénoff, Macrophage-fibroblast circuits in the spleen, Immunol. Rev. 302 (2021) 104–125, https://doi.org/10.1111/imr.12979.

[42] X. Chen, P.B. Comish, D. Tang, R. Kang, Characteristics and biomarkers of ferroptosis, Front. Cell Dev. Biol. 9 (2021), 637162, https://doi.org/10.3389/fcell.2021.637162.

[43] B.R. Stockwell, J.P. Friedmann Angeli, H. Bayir, A.I. Bush, M. Conrad, S.J. Dixon, S. Fulda, S. Gascón, S.K. Hatzios, V.E. Kagan, K. Noel, X. Jiang, A. Linkermann, M. E. Murphy, M. Overholtzer, A. Oyagi, G.C. Pagnussat, J. Park, Q. Ran, C. S. Rosenfeld, K. Salnikow, D. Tang, F.M. Torti, S.V. Torti, S. Toyokuni, K. A. Woerpel, D.D. Zhang, Ferroptosis: A regulated cell death nexus linking metabolism, redox biology, and disease, Cell 171 (2017) 273–285, https://doi.org/10.1016/j.cell.2017.09.021.

[44] J.E. Cassat, E.P. Skaar, Iron in infection and immunity, Cell Host Microbe 13 (2013) 509–519, https://doi.org/10.1016/j.chom.2013.04.010.

[45] E.E. Johnson, M. Wessling-Resnick, Iron metabolism and the innate immune response to infection, Microbes Infect. 14 (2012) 207–216, https://doi.org/10.1016/j.micinf.2011.10.001.

[46] E.J. van Beers, Y. Yang, N. Raghavachari, X. Tian, D. Allen, J.S. Nichols, L. Mendelsohn, S.A. Nekhai, V.R. Gordeuk, J.G. Taylor VI, G.J. Kato, Iron, expression of the pattern recognition receptor-inflammasome system, and early death in adults with sickle cell disease, Blood 124 (2014) 2702, https://doi.org/10.1182/blood.V124.21.2702.2702.

[47] S. Conti, Splenic artery ligation for trauma, Am. J. Surg. 140 (1980) 444–446, https://doi.org/10.1016/0002-9610(80)90187-7.

[48] Q.-M. Wang, Z.-J. Duan, J.-L. Du, S.-B. Guo, X.-Y. Sun, Z. Liu, Heme oxygenase/carbon monoxide pathway inhibition plays a role in ameliorating fibrosis following splenectomy, Int. J. Mol. Med 31 (2013) 1186–1194, https://doi.org/10.3892/ijmm.2013.1309.

[49] S. Potteaux, H. Ait-Oufella, Z. Mallat, Role of splenic monocytes in atherosclerosis, Curr. Opin. Lipidol. 26 (2015) 457–463, https://doi.org/10.1097/MOL.0000000000000223.

[50] T. Aoyama, K. Kuwahara-Arai, A. Uchiyama, K. Kon, H. Okubo, S. Yamashina, K. Ikejima, S. Kokubu, A. Miyazaki, S. Watanabe, Spleen-derived lipocalin-2 in the portal vein regulates Kupffer cells activation and attenuates the development of liver fibrosis in mice, Lab. Invest. 97 (2017) 890–902, https://doi.org/10.1038/labinvest.2017.44.

[51] L. Asher, H. Grossenbacher, The spleen and the metabolism of iron, J. Am. Med. Assoc. LII (1909) 478, https://doi.org/10.1001/jama.1909.02540320050010.

[52] N. Consul, S. Javed-Tayyab, A.C. Morani, C.O. Menias, M.G. Lubner, K.M. Elsayes, Iron-containing pathologies of the spleen: magnetic resonance imaging features with pathologic correlation, Abdom. Radiol. 46 (2021) 1016–1026, https://doi.org/10.1007/s00261-020-02709-x.

[53] A. Kolnagou, Y. Michaelides, C.N. Kontoghiorghe, G.J. Kontoghiorghes, The importance of spleen, spleen iron, and splenectomy for determining total body iron load, ferrikinetics, and iron toxicity in thalassemia major patients, Toxicol. Mech. Methods 23 (2013) 34–41, https://doi.org/10.3109/15376516.2012.735278.

[54] C. Gardi, B. Arezzini, V. Fortino, M. Comporti, Effect of free iron on collagen synthesis, cell proliferation and MMP-2 expression in rat hepatic stellate cells, Biochem. Pharmacol. 64 (2002) 1139–1145, https://doi.org/10.1016/s0006-2952(02)01257-1.

[55] P. Ruytinx, P. Proost, J. Van Damme, S. Struyf, Chemokine-induced macrophage polarization in inflammatory conditions, Front. Immunol. 9 (2018) 1930, https://doi.org/10.3389/fimmu.2018.01930.

[56] M. Navab, S.S. Imes, S.Y. Hama, G.P. Hough, L.A. Ross, R.W. Bork, A.J. Valente, J. A. Berliner, D.C. Drinkwater, H. Laks, Monocyte transmigration induced by modification of low density lipoprotein in cocultures of human aortic wall cells is due to induction of monocyte chemotactic protein 1 synthesis and is abolished by high density lipoprotein, J. Clin. Invest. 88 (1991) 2039–2046, https://doi.org/10.1172/JCI115532.

[57] M. Schnoor, P. Cullen, J. Lorkowski, K. Stolle, H. Robenek, D. Troyer, J. Rauterberg, S. Lorkowski, Production of type VI collagen by human macrophages: a new dimension in macrophage functional heterogeneity, J. Immunol. 180 (2008) 5707–5719, https://doi.org/10.4049/jimmunol.180.8.5707.

[58] F.C. Simões, T.J. Cahill, A. Kenyon, D. Gavriouchkina, J.M. Vieira, X. Sun, D. Pezzolla, C. Ravaud, E. Masmanian, M. Weinberger, S. Mayes, M.E. Lemieux, D. N. Barnette, M. Gunadasa-Rohling, R.M. Williams, D.R. Greaves, L.A. Trinh, S. E. Fraser, S.L. Dallas, R.P. Choudhury, T. Sauka-Spengler, P.R. Riley, Macrophages directly contribute collagen to scar formation during zebrafish heart regeneration and mouse heart repair, Nat. Commun. 11 (2020) 600, https://doi.org/10.1038/s41467-019-14263-2.

[59] A.T. Rowley, V.S. Meli, N.J. Wu-Woods, E.Y. Chen, W.F. Liu, S.-W. Wang, Effects of surface-bound collagen-mimetic peptides on macrophage uptake and immunomodulation, Front. Bioeng. Biotechnol. 8 (2020) 747, https://doi.org/10.3389/fbioe.2020.00747.

[60] A.M.H. Larsen, D.E. Kuczek, A. Kalvisa, M.S. Siersbæk, M.-L. Thorseth, A. Z. Johansen, M. Carretta, L. Grøntved, O. Vang, D.H. Madsen, Collagen density modulates the immunosuppressive functions of macrophages, J. Immunol. 205 (2020) 1461–1472, https://doi.org/10.4049/jimmunol.1900789.

[61] P. Krzyszczyk, R. Schloss, A. Palmer, F. Berthiaume, The role of macrophages in acute and chronic wound healing and interventions to promote pro-wound healing phenotypes, Front. Physiol. 9 (2018), https://doi.org/10.3389/fphys.2018.00419.

[62] M. Kobayashi, T. Suhara, Y. Baba, N.K. Kawasaki, J.K. Higa, T. Matsui, Pathological roles of iron in cardiovascular disease, Curr. Drug Targets 19 (2018) 1068–1076, https://doi.org/10.2174/1389450119666180605112235.

[63] D.P. Dyer, K. Pallas, L. Medina-Ruiz, F. Schuette, G.J. Wilson, G.J. Graham, CXCR2 deficient mice display macrophage-dependent exaggerated acute inflammatory responses, Sci. Rep. 7 (2017) 42681, https://doi.org/10.1038/srep42681.

[64] S. Fox, A.E. Leitch, R. Duffin, C. Haslett, A.G. Rossi, Neutrophil apoptosis: relevance to the innate immune response and inflammatory disease, J. Innate Immun. 2 (2010) 216–227, https://doi.org/10.1159/000284367.

[65] K. Asagoe, K. Yamamoto, A. Takahashi, K. Suzuki, A. Maeda, M. Nohgawa, N. Harakawa, K. Takano, N. Mukaida, K. Matsushima, M. Okuma, M. Sasada,

Down-regulation of CXCR2 expression on human polymorphonuclear leukocytes by TNF-alpha, J. Immunol. 160 (1998) 4518–4525.
[66] I. Tikhonov, T. Doroshenko, Y. Chaly, V. Smolnikova, C.D. Pauza, N. Voitenok, Down-regulation of CXCR1 and CXCR2 expression on human neutrophils upon activation of whole blood by S. aureus is mediated by TNF-alpha, Clin. Exp. Immunol. 125 (2001) 414–422, https://doi.org/10.1046/j.1365-2249.2001.01626.x.
[67] L. Franken, M. Schiwon, C. Kurts, Macrophages: sentinels and regulators of the immune system, Cell. Microbiol. 18 (2016) 475–487, https://doi.org/10.1111/cmi.12580.
[68] D. Kurotaki, T. Uede, T. Tamura, Functions and development of red pulp macrophages, Microbiol. Immunol. 59 (2015) 55–62, https://doi.org/10.1111/1348-0421.12228.
[69] J.A. Araujo, M. Zhang, F. Yin, Heme oxygenase-1, oxidation, inflammation, and atherosclerosis, Front. Pharmacol. 3 (2012) 119, https://doi.org/10.3389/fphar.2012.00119.
[70] J.J. Boyle, M. Johns, J. Lo, A. Chiodini, N. Ambrose, P.C. Evans, J.C. Mason, D. O. Haskard, Heme induces heme oxygenase 1 via Nrf2, Arterioscler. Thromb. Vasc. Biol. 31 (2011) 2685–2691, https://doi.org/10.1161/ATVBAHA.111.225813.
[71] T. Nguyen, P. Nioi, C.B. Pickett, The Nrf2-antioxidant response element signaling pathway and its activation by oxidative stress, J. Biol. Chem. 284 (2009) 13291–13295, https://doi.org/10.1074/jbc.R900010200.
[72] K. Hadian, B.R. Stockwell, SnapShot: ferroptosis, Cell 181 (2020), https://doi.org/10.1016/j.cell.2020.04.039, 1188-1188.e1.
[73] V. Fernández-García, S. González-Ramos, P. Martín-Sanz, A. Castrillo, L. Boscá, Contribution of extramedullary hematopoiesis to atherosclerosis. the spleen as a neglected hub of inflammatory cells, Front. Immunol. 11 (2020), 586527, https://doi.org/10.3389/fimmu.2020.586527.
[74] C. Xu, S. Sun, T. Johnson, R. Qi, S. Zhang, J. Zhang, K. Yang, The glutathione peroxidase Gpx4 prevents lipid peroxidation and ferroptosis to sustain Treg cell activation and suppression of antitumor immunity, Cell Rep. 35 (2021), 109235, https://doi.org/10.1016/j.celrep.2021.109235.